 doi:10.20944/preprints202101.0556.v1

Article

The One-way FSI method based on RANS-FEM for the Open Water Test of a Marine propeller at the different advance coefficient

Mobin Masoomi [1], Amir Mosavi [2,3,*]

[1] Department of Mechanical Engineering, Babol Noshirvani University of Technology, Babol, Iran;
[2] Faculty of Civil Engineering, Technische Universität Dresden, 01069 Dresden, Germany
[3] Norwegian University of Life Sciences, Oslo, Norway
* Correspondence: amir.mosavi@mailbox.tu-dresden.de

Abstract: This study addressed a Fluid-Structure Interaction (FSI) of an open Water test for vp1304 propeller to predict pressure and stress distributions with a low cost and high precision method. The most prominent method (one-way coupling) uses one hydrodynamic solution for the number of different structural sets involved in other materials or different layup methods or layers' combination. An open-access software (OpenFOAM) with an open-source code solver simulates the fluid domain. Abaqus is used To evaluate and predict the blade's deformation and strength with the Finite Element Method (FEM). The coupling approach is based on dry condition, which means the added mass effects due to propeller blades vibration is neglected. The pressures imposed on the blades are extracted from the fluid solver for each time-step. Then, These pressures role as a load condition for the structure solver. This approach was verified (wedge impact); a key factor for the present solution is the rotational rate interrelated between two solution domains, which is explained in this paper. Finally, the blades' stress and strain are calculated and compared in each advance coefficient.

Keywords: Fluid-Structure Interaction; OpenFOAM; One-way approach; Structural Analysis; Open Water Test

1. Introduction

The propeller is the main part of a propulsion system by which engines' power can move the marine vessels. Marine propellers work in a heavy and complicated flow field and high-risk work conditions; thus, two aspects must be considered to design a new propeller. First, evaluating the hydrodynamic coefficients like efficiency and thrust and torque coefficient. Second, strength due to loads and manufactured material. The propeller blade strength role is essential in the cavitation phenomenon and propellers' efficiency. In essence, the blades' structural Behavior has fully interacted with the propulsion systems' hydrodynamic qualification, particularly propeller efficiency. There were two main approaches for hydrodynamic calculation of marine propeller: the first inviscid numerical methodologies involved, the lifting line method, the boundary element method (BEM)[1] and the vortex lattice method (VLM)[2], and Second is computational fluid dynamic (CFD) that involves some techniques like large eddy simulation (LES)[3], Reynolds averaged Navier Stokes(RANS) [4-6]On condition that marine propeller operates in a viscous flow and complex current of wake induced. Although The CFD methods are more suitable and efficient than the inviscid methods (BEM, VLM), some researchers use the inviscid method for propeller simulation due to the low cost and lower simulation power needed.

Many researchers used the RANS method to solve the rotating blades like a marine propeller, Abdel Maksoud et al.[7], carried out on how the propeller hub could change the propeller efficiency by using CFX. Moreover, another main factor in marine propeller operational condition is the interaction of propeller and rudder, Simenson et al. [8] researched in this field by coupling RANS and

 doi:10.20944/preprints202101.0556.v1

potential flow. Valentine [9] used the RANS equations to predict the propeller blades' flow characteristics by considering turbulence inflow characteristics. In this paper, two main issues should be evaluated, first hydrodynamic calculations based on Reynolds averaged Navier–Stokes method for a propeller(vp1304). Second, structural Analysis, fluid-structure interaction must be engaged in the computational prediction approach. The nonlinear hydrodynamic load exerted on propeller blades due to the propeller's rotational motion inducing a centrifugal force.

The majority of fluid-structure interaction studies on marine propeller focus on the composite propeller; Das et al. [10] used a reverse-rotation propeller in a CFD analysis. Mulcahy [11] investigated a comprehensive study on the composite propellers' hydro-elastic tailoring. In 2011, blasques et al. [12] studied how laminate layup of the marine composite propeller can simultaneously decrease fuel consumption, whereas increases in the vessel's cruise speed. In 2008 [7], Young carried on fluid-structure interaction analysis of marine propeller to assess the composite blade's Behavior in a work condition. Also, the Tsai-Wu strength criterion is considered to evaluate the blade strength. Hyoungsuk lee et al. [13] investigated two-way coupling FSI analysis consisting of added mass based on the coupling between boundary element and finite element method. X.D.He et al. [14] used a hydro-elastic approach to evaluate composite propeller's performance, especially vibration due to loads on propeller Hub and the composite layup scheme. This approach was shaped base on coupling CFD and FEM methods. Finally, a comprehensive study for four propellers with different concerning materials was published in 2018 by Maljars et al.[15], which consist of RANS-FEM and BEM–FEM results against experimental results.

The present study approach introduces a simple FSI surrogate modeling by considering two distinct solvers, Linux based/open access solvers (OpenFOAM) with windows based/commercial software (Abaqus). The major challenge and novelty of the represented approach is how two solvers could connect without any in-house code besides high-fidelity results. These method types are barely discussed, particularly for marine propellers' open water tests. In the following sections, for the first step hydrodynamic solution verified with experimental tests. as well as for the structural solution, the present FSI approach compared with wedge impact case which was verified later, the justification of using the wedge impact verification is the similarity of two cases. For the second step, the verified numerical model performs to analyze the advance coefficients' effect on the forces and stresses imposed on the propellers' blade.

2. Materials and Methods

FSI numerical models' solution approach is divided into the monolithic and partitioned method. Partitioned methods are divided into the one-way and two-way approach. Moreover, two-way coupled is further divided into strong and weak, Vaassen et al. [16]. As for the accuracy aspect, The two-way coupling approach is more accurate than the one-way, especially for the cases with bigger and more considerable deformations. On the other hand, the one-way coupled requires data for a single iteration per time-step, Friedrich-Karl Benra et al. [17] .Thus, the time needed for analyzing is lower than two-way coupling, which is updated after each time-step for a new iteration. Therefore, An advantage of the one-way approach is decreasing the numerical solution time. The second advantage is that the mesh advocated for the fluid domain does not need to be re-calculated at each time-step. This leads the numerical solution to remain stable unchanged mesh quality. By considering the result of Dominic J. Piro Ph.D. thesis 2013 [18], which compares the accuracy of a one&two-way coupling approach(RQS-RDyn-TC) for different plate thicknesses. The results indicate that the diagrams were close to each other for a thick plate with low deformation. In this study, the one-way coupling method could be accurate enough for the present case(in this case: vp1304 model), which has a small deformation.

2.1.Governing Equations Of The Flow Around The Propeller

The propeller's fluid is considered an incompressible Newtonian that should inherently satisfy the mass conservation equation and momentum, which involved Navier-stokes equations(N-S) or

Preprints (www.preprints.org) | NOT PEER-REVIEWED | Posted: 27 January 2021 doi:10.20944/preprints202101.0556.v1

Reynolds Average Navier Stokes equation(RANS) for the turbulent regime. interFoam is a solver based on the RANS equation by considering many turbulence models [19].

$$\frac{\partial u_i}{\partial x_i} = 0 \tag{1}$$

$$\frac{\partial (u_i)}{\partial t} + \frac{\partial (u_i u_j)}{\partial x_j} = f_i - \frac{1}{\rho}\frac{\partial p}{\partial x_i} + \frac{\partial}{\partial x_j}\left[v\left(\frac{\partial u_i}{\partial x_j} + \frac{\partial u_j}{\partial x_i}\right) + \tau_{ij} \right] \tag{2}$$

where $x_i = (x,y,z)$ represents coordinates, $U_i = (U,V,W)$ are the component of Reynolds-Averaged velocity. f_i denotes the body forces presented as forces per unit volume and in the present study assumed that $f_i = 0$. moreover, u, ρ, and P are fluid velocity vectors, density, and pressure, respectively. The Boussinesq assumption is considered To represent the Reynolds stress for incompressible flows, which is commented below:

$$\tau_{ij} = \upsilon_t \left(\frac{\partial u_i}{\partial x_j} + \frac{\partial u_j}{\partial x_i} \right) - \frac{2}{3}\delta_{ij} k \tag{3}$$

$$k = \frac{1}{2}\left((\overline{u}')^2 + (\overline{v}')^2 + (\overline{w}')^2 \right), \quad u' = u - \bar{u}, \quad \bar{u}' = \frac{1}{T}\int_0^T (u(t) - \bar{u})dt \tag{4}$$

Where ν_t represent the eddy viscosity, k denotes turbulent kinetic energy per mass(TKE). Also, δ_{ij}surrogate as the Kronecker symbol. U is the instantaneous and $\bar{u}$ is average velocity, in which $\overline{u'}$ and $(\overline{u'})^2$ are the mean and variance velocity, respectively. A two-equation turbulence model, k-ε, is used for the present study. ε denotes the dissipation rate of energy in turbulence regime per mass, Which determines the amount of energy lost by the viscous forces in the turbulent flow should be introduced. (μ_t) is turbulent viscosity.

$$\mu_t = \rho C_\mu \frac{k^2}{\varepsilon} \tag{5}$$

$$\varepsilon = \frac{1}{2}\frac{\mu}{\rho}\overline{\{\nabla u' + (\nabla u')^T\} : \{\nabla u' + (\nabla u')^T\}} \tag{6}$$

To track the particles and capture the interface for the multi-phase solution easily, the Volume Of Fluid(VOF) could be an effective approach. The VOF method uses a volume fraction variable α to represent the water fraction in each finite volume cell [20]. Where $\rho_1$and μ_1 represent the physical properties of fluid1(water), and ρ_2 and μ_2 also mean the physical properties of fluid2(air). This approach introduces a new conservation equation that must be solved for each time-step.

$$\rho = \alpha\rho_1 + (1-\alpha)\rho_2 \qquad \mu = \alpha\mu_1 + (1-\alpha)\mu_2 \quad , \quad \begin{matrix} \alpha{=}0 & \text{:air} \\ \alpha{=}1 & \text{:water} \end{matrix} \tag{7}$$

The two-phase dynamic solution similar to the present case(propeller rotation in water) is a transient case with a high turbulent regime, and the solution is inherently unstable. Thus, the high-fidelity algorithm based on PIMPLE's implicit solution is used to couple the mass conservation and momentum equations. This algorithm merges SIMPLE(Semi-Implicit Method for Pressure-Linked Equations) and PISO (Pressure Implicit with Splitting of Operators). The Courant number is automatically changed due to grid resolution and the method's stability, but there are two important parameters, inner and outer correctors. Inner corrector is the number of times the pressure is corrected, and outer corrector is belonged to how many times the equations are solved in each time-step. Outer corrector puts an obligation to stop the solution for each time-step apart from the solution be converged or not.

Preprints (www.preprints.org) | NOT PEER-REVIEWED | Posted: 27 January 2021 doi:10.20944/preprints202101.0556.v1

2.2. Governing The Structural Equations

In FSI problems, structural analysis is an essential step that should be performed correctly. The cantilever beam model is the initial theory to calculate the propeller blade strength introduced by Taylor(1933)[21]. This method was implemented and developed by some researchers. The drawback of th method was poor results for the points with a low thickness on the propeller's blade in contrast with the points near the propellers' root. This problem continued until the introduction of shell theories developed by Cohen[22] and Conolly[23]. The limitation of this method was the propellers' geometry complexity. For instance,The wide blade or high skew propellers could not be assessed accurately. In recent years, the finite element method has been used widely in improving the computer's calculation power. This method is substantially divided into solid or shell element approaches. Many investigations are based on both approaches, but young[24] and Blasques et al. [12] performed a study to evaluate the output results' differences. Their investigation indicates that, although both methods are sufficient, the Shell element model needs lower computational power than the solid element method. Moreover, the solid element method has some prominency rather than a shell element model (Young [24]. This is why most FSI problems used a solid element model for structural solver.

The calculation for the structure part is performed using the finite element method. The deflection that occurred because of the imposing load on the structure is The main issue in structural simulation [25]. The technique broadly consists of discretizing a structure into several elements that must then assembled. However, Due to the continuity of stress for interface elements, internal stresses in equilibrium. FEM used the Explicit method as the CFD part of the solution, in which a time-based approach(central difference method) is used to integrate the motions' Equation. In this method, the period is considered small enough to prevent divergence. [26]. The Equation of motion for the structural deformation corresponding to the propeller blade fixed coordinate is introduced by Equation (8).

$$M_s\ddot{d} + C_s\dot{d} + K_s d = F_{ST} \tag{8}$$

Where M_s is the mass matrix, C_s belongs to damping matrix and K_s represent the matrix for the structure stiffness. the variables($\ddot{d}, \dot{d}, d$) are the acceleration, velocity, and displacement, respectively. (F_{ST}) is the summation of all loads imposed on the structure. Substantially for the cases like a propeller, this load comprises force due to rotation, centrifugal force and moments, Coriolis force, and finally external load on the structure. For the case in hand, due to static Analysis of the propeller and motionless blades in each time-step, the only pressure used for calculation is the fluid pressure extracted from the CFD solution. The calculation algorithm's first step is to solve the dynamic equilibrium relation, Equation (9). The kinematic conditions solve the next iteration's kinematic constraint in each distinct increment.

$$\ddot{U} = (M)^{-1}(P - I)_t \quad , \quad M\ddot{U} = P - I \tag{9}$$

$$\dot{U}_{(t+\frac{\Delta t}{2})} = \dot{U}_{(t-\frac{\Delta t}{2})} + \frac{(\Delta t_{(t+\Delta t)} + \Delta t_{(t)}}{2}\ddot{U}_t \tag{10}$$

$$U_{(t+\Delta t)} = U_{(t)} + \Delta t_{(t+\Delta t)}\dot{U}_{(t+\frac{\Delta t}{2})} \tag{11}$$

All of these parameters are belong to nodal points, Where M is the nodal mass matrix, U is nodal displacement and $\ddot{U}$, is nodal acceleration. To govern net forces act on nodal points, (P-I) is used, That (p) is the external loads imposed on the structure. This parameter is considered as nodal forces. The integrated accelerations are used to calculate velocity variations; this new added velocity value from the previous middle increment to determine the velocities at the middle of the current increment equation(10), then The time-integrated velocities are added to the beginning displacements' increment to determine the final displacements' increment, equation(11); After estimation of the nodal displacement in time(t), the element strain increments, are calculated from the strain rate, The

Preprints (www.preprints.org) | NOT PEER-REVIEWED | Posted: 27 January 2021 doi:10.20944/preprints202101.0556.v1

stress components can be calculated from constitutive equations and the solution process repeated for time t+Δt.

2.3. Modeling And Computational Setup

2.3.1. Open Water Test Characteristic

The present study's framework is presented as a numerical solution for the Potsdam propeller test case(PPTC). Thus, the same propellers' geometry with the same material is accepted for the surrogate modeling, represented in Table 1 and Table 3, repectively[27]. As recommended by the ITTC(The International Towing Tank Conference), the propeller rotational speed considered a constant value for a particular open water test, but the propellers' advanced speed varies. The inlet water is in opposite rather real condition; thus, the propellers must be rotated in the opposite direction. We will hereafter comply with this rule to perform open water tests in the present study. The solution domain is modeled cylindrically with the following dimensions; (3.5D forward, (10D rearward), and (5D in diameter), D is propeller diameter [28], these dimensions are shown in Figure 1.

Table 1. geometrical specification of the propeller

Propeller model	Vp1304
Diameter	0.25m
Hub coefficient	0.3
Num. Blades	5
pitch coefficient *(r/R=0.7)*	1.635
A_E /A_0	0.779

Table 2.Structural specification of the propeller

Material	Al-Alloy
Elasticity	120 Gpa
Poisson's Ratio	0.34
Mass Density	7400

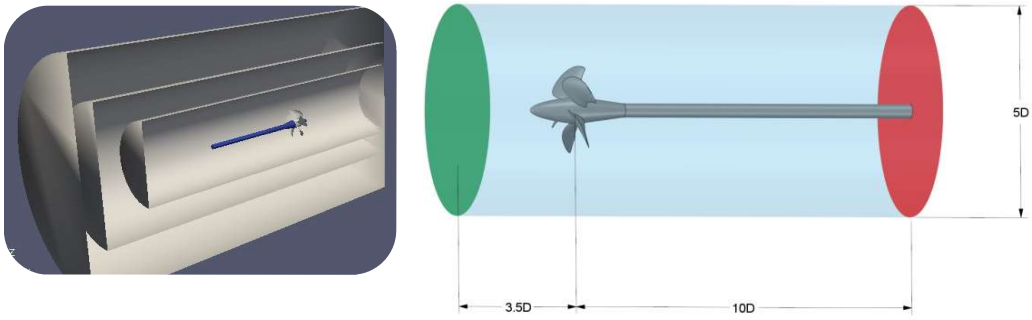

Figure 1.Numerical solution domain used for the present study

The main parameter at open water tests are the thrust coefficient (k_t), and torque coefficient(k_Q) could be represented by the dimensionless values mentioned in equation 15. These coefficients are directly related to rotational speed (n), diameter(D) of the propeller, and water density(ρ). where: (T – thrust [N])- (Q – torque [Nm])- (V_a– advance speed [m/s]- (η= efficiency[-]).

Preprints (www.preprints.org) | NOT PEER-REVIEWED | Posted: 27 January 2021 doi:10.20944/preprints202101.0556.v1

$$J = \frac{V_a}{nD} \qquad k_t = \frac{thrust}{\rho n^2 D^4} \qquad Kq = \frac{Torque}{\rho n^2 D^4} \qquad \eta = \frac{K_T J}{2\pi K_Q} \tag{12}$$

2.3.2. Applied Boundry Condition And Dynamic motions Method

Various boundary conditions can be deployed to the numerical solutions, but good results without divergence need an appropriate one. the inlet&outlet were set at the downstream of the domain into OutLet boundary. For Inlet boundary condition, free-flow velocity is considered constant, dependent on advance velocity for each advance coefficient. Moreover, the inlets' turbulence intensity is regarded as 1%. Two main approaches could simulate the propeller's dynamic motions, Multi Reference Frame(MRF) and Arbitrary Mesh Interface (AMI). Since the AMI is more practical for propeller cases, it is used as a dynamic solution approach in this study. This method is based on the interpolation between two distinct but adjacent domains connected with an interface [29]. Two similar cylindrical domains encompass the propeller, one is static, and another one is dynamic, which moves with the propeller. Although there was no physical relationship between the two zones, the fluid and numerical results were transported with the interface between them. The wall boundary condition assigned for the propeller blade and the Hub was rotational, with a zero velocity for the adjoining cell zone.

Three-sized cylindrical shape zones are generated To have a structural-based mesh with an appropriate mesh quality around the propeller. The smallest cylinder has a small grid size, and the subsequent cylinder has a larger gride size compared with the former. In this regard, snappyHexMesh was used as the main tool and rhinoceros' role as an assistant tool for griding the numerical solution domain. As shown in Figure 2, a high-quality structured mesh can be obtained by considering these techniques. A mesh independence study establishes the CFD solutions' accuracy and keeps the computational cost-efficient.

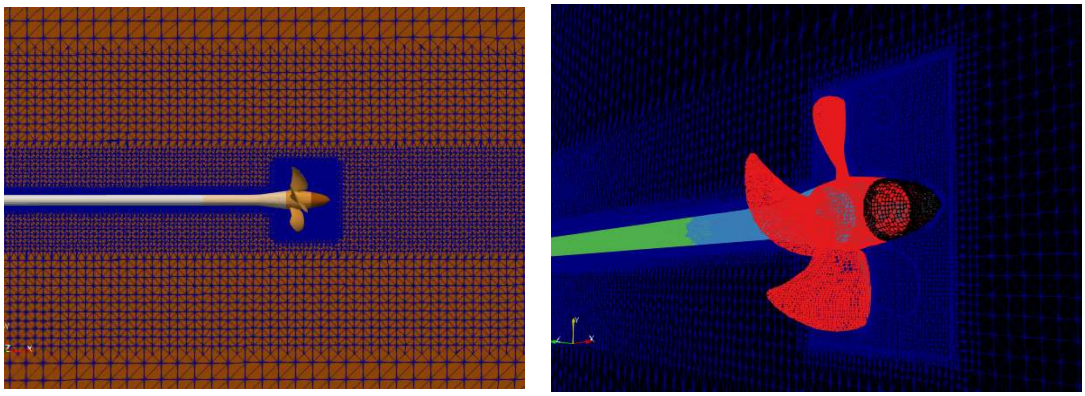

Figure 2. Mesh generated structure around the propeller

The mesh generation framework is explained, but mesh independence must be performed simultaneously. The mechanism whereby the performance of griding qualified is highly dependant on the main propeller characteristics shown in Equation (12); that's how the mesh could be alleviated the computational cost without losing the accuracy. A case with the propeller rotational speed (ω=15 rps), the propeller advance speed(v_a=2 m/s) Finally, the advance coefficient(J=0.53[-]) is considered. The numerical solution performs for five distinct cases with the condition shown in Table 3 and initial values except for the griding size. For the case in-hand, InterDyMFoam is a solver for dynamic multi-phase solutions selected among OpenFOAM libraries with the same underlying physics into InterFoam. The thrust and Torque are extracted from the post-processing tool for OpenFOAM as the initial value, then these values placed in the relations of Equation (12), and finally the results for each simulation gathered in Table 4; all these cases provided acceptable results, with less than e=11% error

Preprints (www.preprints.org) | NOT PEER-REVIEWED | Posted: 27 January 2021 doi:10.20944/preprints202101.0556.v1

for the coarse mesh. Consequently, Fine(IIII) resolution leads to a reasonable prediction of thrust and torque coefficient with optimum computational cost compared with other cases.

Table 3. Primary data assumed in calculations

parameter	unit	Model	real
Density (water)	kg m^{-3}	999.0	1025
Kinematic viscosity (water)	m^2 s^{-1}	1.139e-6	1.188e-6
Rotations(propeller)	s^{-1}	15	4.33

Table 4. Mesh independency study for vp1304 propeller

NUM	quality	Base Grid	Cell.NUM	$\frac{k_t}{(k_t)_{excellent}}$	$\frac{k_q}{(k_q)_{excellent}}$
(I)	Coarse	0.11	245210	1.1	1.11
(II)	Mid	0.09	315402	1.05	1.055
(III)	Mid-fine	0.08	335183	1.025	1.024
(IIII)	Fine	0.064	425060	1.015	1.013
(V)	Excellent	0.0325	835205	≈1	≈1

3. Results and Discusion

3.1.CFD Validation

The numerical model tests were performed the same as the experimental tests[30]; with advances coefficient shown in

 doi:10.20944/preprints202101.0556.v1

Table **5**. As before said, only the cylinder around the propeller rotates; thus, apart from this domain, others are static without any dynamic motion. Based on Figure 3 (right), the best resemblance between the present results and the experiment results belongs to efficiency(η), with an average e=4%. The question is why the results for the Torque coefficient (k_q) are not as good as other variables; the initial impression is that the rotating parts involved shaft, the electric machine is not equal between experiment and numerical solution. To some extent, these errors are unavoidable, but the overall results show a good resemblance. Another important factor affecting the results is the turbulent regime; as can be seen, Due to severe turbulence flows around the propeller, the maximum error percentage belongs to J=0.266(near bollard state) with the highest turbulent rate. Neither this numerical method nor any other methods could acquire good results for low advance coefficients. That is why the e=20%-30% error is an intrinsic part of the simulation, especially for low advance coefficients. Thus, the J=0.266 error percentage does not involve in average error calculation. Finally, e=3.85% is considered as the average error percentage for the present method. A complete circumstance of error changes for three main propellers' factors is shown in Figure 3(left).

Preprints (www.preprints.org) | NOT PEER-REVIEWED | Posted: 27 January 2021 doi:10.20944/preprints202101.0556.v1

Table 5. different advance coefficient specification

Num	J(-)	ω(rps)	V_a(m/s)
I	0.266	15	1
II	0.533	15	2
III	0.8	15	3
IIII	1.06	15	4
V	1.23	15	5
VI	1.6	15	6

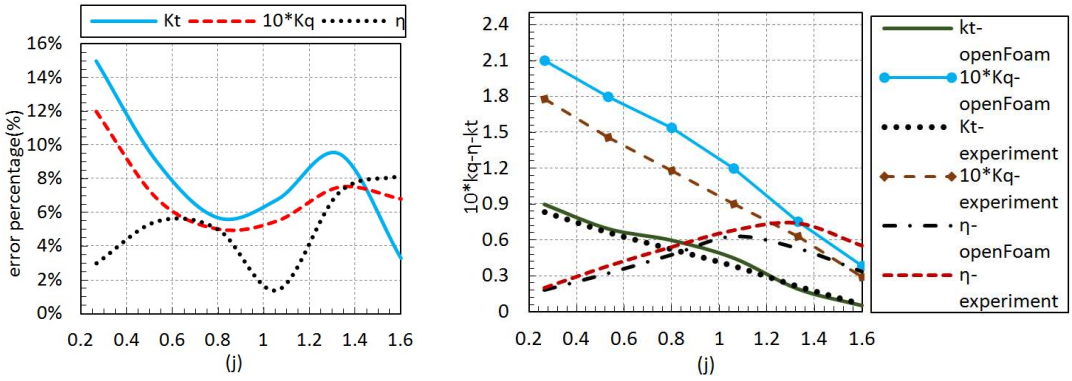

Figure 3. Compare between experimental and numerical results, model scale(right), error percentage(left)

3.1.1. Hydrodynamic Analysis Of The vp1304 Propeller

Four advance coefficient related contours are illustrated in Figure 4 to show how the particles move around the propeller field; However, the emphasis is on faces and backside propellers' pressure; the general increasing the pressure field around the propeller could be considered for quantitative analysis. In essence, for the bigger advance coefficient, The blade's pressure gradient decrease. This leads the propeller's thrust and Torque to be lower than the bigger advance coefficient. That is why the maximum propeller's thrust occurred at Bollard state(advance velocity=0), and after that, gradually decrease until it reaches near-zero for j=1.6 onwards. Because The pressure and velocity are related to each other, evaluation of the flow field, and the velocity attitude must be considered. The discrepancies between j=0 and j=1.23(minimum and maximum advanced coefficient) for velocity contour are involved in the fluid flow sequence's value and shape. As the advance velocity increases, the propellers' backflow becomes more parallel with low dispersion, And the velocity be smoother around the propeller; accordingly, the hydrodynamic gradient pressure for propeller blades decreases.

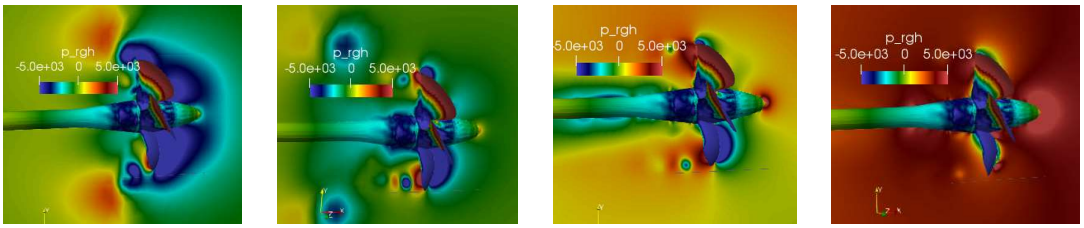

Preprints (www.preprints.org) | NOT PEER-REVIEWED | Posted: 27 January 2021 doi:10.20944/preprints202101.0556.v1

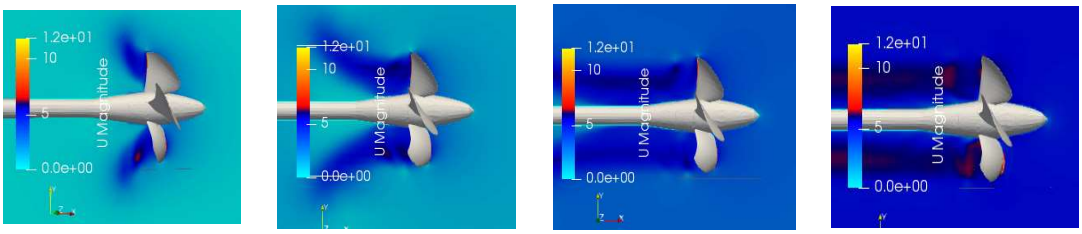

(J=0) (J=2.66) (J=0.8) (J=1.23)

Figure 4. pressure(top) and velocity(bottom) contour for different advance coefficient

For an in-depth analysis of how the propellers' blades pressure changed, three pressure gauges(p-1/p-2/p-3) shown in Table 6 are considered on the propeller surface to record the outputs pressure. As shown in Figure 5, for p-1(near the blade root), the pressure values apart from the advance coefficient are in a closed interval. This trend is somewhat true for p-2(middle of blades), but for p-3(near the leading edge), the value for j=0 and j=1.266 are almost six times than j=1.26. The increasing rate for pressure is so sensitive for the leading edge points. However, the utmost diagram trends are linear for different advanced coefficients; for j=0.8, the pressures' variations are not in an approximate line and have diagram extremums.

Table 6. three gauges position on propeller blade

gauge	Distance from the center
p-1	0.04m
p-2	0.08m
p-3	0.12m

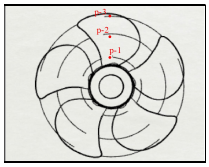

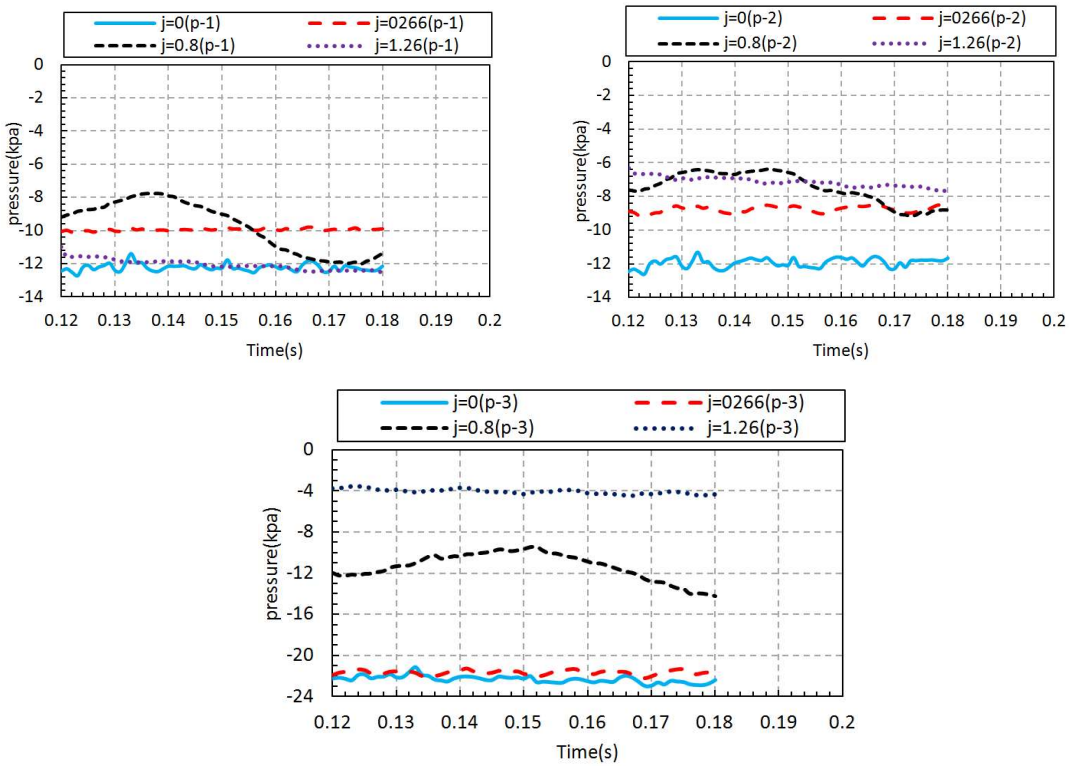

Figure 5.gauge pressure variations of one rotation(t=0.12s-t=0.18s) for different advanced coefficient

Preprints (www.preprints.org) | NOT PEER-REVIEWED | Posted: 27 January 2021 doi:10.20944/preprints202101.0556.v1

A valid question is how the force imposed on the propeller changed. This question was answered by following the same approach of pressure evaluation. Upon this, ParaView, a visualization and post-processing tool for OpenFOAM, is accomplished for force evaluation. A framework for the force solution is generated and captured each propeller blade surface and adopted normal vectors on these surfaces. After that, by multiplying the pressure with these normal vectors, the force could be extracted from the hydrodynamic solution. There is another method for analyzing the imposed force by accomplishing FORCE-Library from the OpenFOAM package. The drawback of this method is, the solved solution within this package must start from the beginning of the simulation. As predicted, the maximum force imposed on the propeller occurred at J=0, shown in Figure 6; also, the smallest advance coefficient J=0.266 experienced the force(F=600 N) similar to the value for Bullard Pull(J=0).

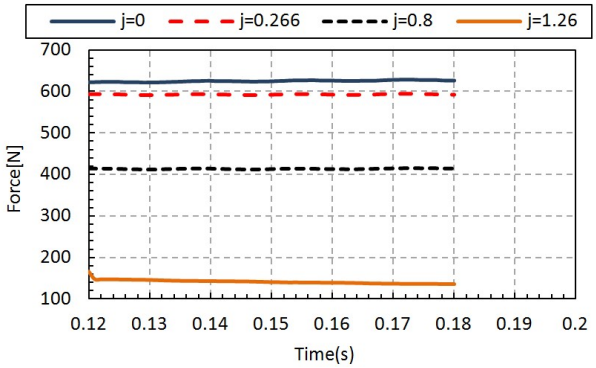

Figure 6. integral forces act on the propeller at the different advanced coefficient

3.2. *Fluid-Structure Interaction Validation*

3.2.1. Finite-Element Method

The acquisition of Von-Mises stress is at scope coverage of the present method by implementing the static/general solution of Abaqus solvers. Substantially the propeller's dynamic motions are only considered in the CFD approach, and it is reasonable to suppose that the propeller is fixed at the propeller stem for each time-step of the structural solver. As before said, The FEM solver used solid elements with three translation degrees of freedom, the displacements, and rotations (u, v, w, ϕ_1, ϕ_2}. Moreover, weight functions (δu, δv, δW_1, δw_2, δw_3) are approximated:

$$u = \sum_{j=1}^{n} u_j.\psi_j \quad , \delta u = \psi_i \qquad \varphi_1 = \sum_{j=1}^{n} w^2{}_j.\psi_j \quad , \delta w_2 = \psi_i$$

$$v = \sum_{j=1}^{n} v_j.\psi_j \quad , \delta v = \psi_i \qquad \varphi_2 = \sum_{j=1}^{n} w^3{}_j.\psi_j \quad , \delta w_3 = \psi_i \qquad (13)$$

$$w = \sum_{j=1}^{n} w_j.\psi_j \quad , \delta w_1 = \psi_i$$

These Lagrange interpolation functions(ψ_i)are substituted in the differential equations' weak form [31]. These are functions of nodal parameters(x and y) in which x and y are nodal displacements. At the finite element methods based on displacement, the displacements' manner in the element boundaries is not separated, but the strains are (13). The manner of strain is continuous only within one element. The point is, choose between the linear or quadratic elements. Indeed, the strains have a constant value in linear elements, but in quadratic elements, the strains are nonlinear with more accurate strain(or stress) results than linear elements. According to Barlow [32],[33]. Strains and stresses can be solved without limitation in the element, just for points including defined nodes.

Preprints (www.preprints.org) | NOT PEER-REVIEWED | Posted: 27 January 2021 doi:10.20944/preprints202101.0556.v1

3.2.2. One-Way Coupling Approach

In the present paper, the primary purpose is to study the influence of the 'advance coefficient' on the propellers' structural response; within a one-way coupling approach. There are two main modes(Dry&Wet modes) with the key factor of 'added mass-generated effects' due to structural deformations. Dry condition considers only material/structural damping and wet condition consider added mass due to the blades' vibration. Wet modes are computed by Finite Element embedding the structure in a fluid domain modeled by acoustic elements. When the propeller reaches maximum load at real state condition, blades begin to vibrate on their natural frequencies. In fact, Analysis under "wet" conditions can give more accurate and reliable results, especially for large deformations. Due to the investigation of Hyoungsuk Lee et al. [13], The difference between the results of the dry and wet conditions is not significant for the case with low deformations. The one-way coupling with the dry condition has been used in the present study. The underlying physics dominant on the one-way coupling is, fluctuating quiddity due to large deformation and membrane forces; thus, The diagrams experienced large oscillations; this procedure was verified with wedge impact case.

An aluminum wedge's results are considered and verified with the results of Agards' and pancirolis' investigation [34]To evaluate the model's applicability. The wedge characteristic used for the numerical solution is shown in Table 7; two variables were considered, von-Mises stress and strain, to verify the results. Since the most extensive and biggest values of these variables occurred at the midpoint of the wedge wing(150mm from wedge apex) at the interior side(1mm above the neutral axis) and whatever as the deformations are more intensive than other points, the precision and accuracy of the one-way approach become lower; thus the selection of this point is due to challenging the method under the most complicated mode. The diagrams are shown in Figure 7.present method(by considering the wedge impact) verification versus two-way couplig, verified with Agard[20]. This process is valid due to the similarity of steps and methods for the present study and can be reliable enough to use as a base approach of the vp1304 propeller. With this justification, this process verified for wedge impact can be utilized to analyze vp1304 propeller with a small but important amended step; This involved the rotation of propeller at each time-step for the structural solver, which is discussed further in the next sections.

Table 7.wedge characteristic used for one-way coupling verification solution

characters	Wedge length	Wedge thickness	Deadrise Angle
value	0.3 m	0.002m	20(degree)

characters	Wedge material	E [Gpa]	ρ[kg/m^3]	ν [-]
value	Aluminum	68	2700	0.3

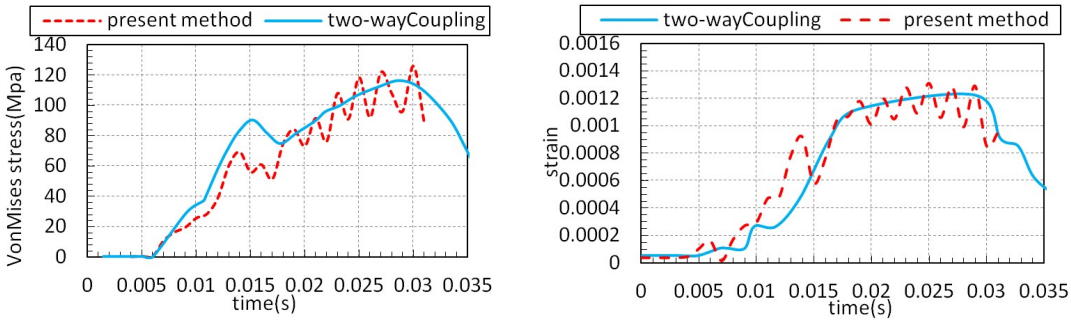

Figure 7.present method(by considering the wedge impact) verification versus two-way couplig[20]

Preprints (www.preprints.org) | NOT PEER-REVIEWED | Posted: 27 January 2021 doi:10.20944/preprints202101.0556.v1

In the present study, an approximation for fluid-structure interaction is called rigid/quasi-static (RQS), in which the structure is considered as a rigid body for fluid simulations. Also, the flexural mass is neglected in RQS approximation. Thus, the forces due to hydrodynamic pressure are independent against the structure deformation. In Equation(14), $f_R(t)$considered as the fluid force and The deformations(δ_{RQS}) extracted from this method are always smaller than the real deformations. Thus, as said in Heller and Jasper [35], a "dynamic amplification factor" must be applied due to neglecting the flexural mass to correct error predicting. As shown in **Figure 8**, the one-way coupling is used as the leading solution approach. Initially, the fluid domain is solved by InterDyMFoam, which is thoroughly explained in the next section. After that, the pressures act on propeller blades is captured and saved as an excel file for every time-steps. These pressures role as a structural load in the Abaqus load condition module. The main point is, in every time-steps, the propeller must have a proportional rotation. In return for any rotation angle for the propeller in the fluid domain, the same angle must be considered in the structural part. Thus, blades in the structural solver need to change upon rotation angle. The rotation angle is related to angular frequency(ω). The value for rotation angle at each time step can be easily obtained. By considering the equation 15(a), the time for one complete rotation(T) can be obtained; 15 (b) shows the number of angular advance per each time-step. Finally, 15(c) shows the rotation angle at each time-step.

$$k.\delta_{RQS} = f_R(t) \tag{14}$$

(a), $\omega = \frac{2\pi}{T}$ (b), $n = \frac{\nabla t}{T}$ (c), $m = \frac{360}{n}$ (15)

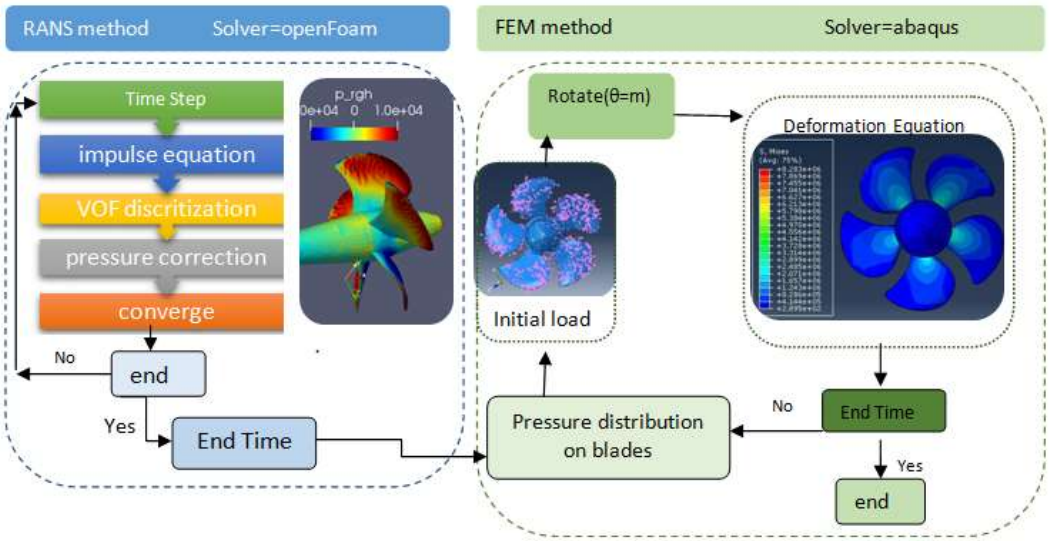

Figure 8. The comprehensive chart of the present method by considering the solvers engaged

Apart from some exceptions, Maximum stress occurred near the blades' root, and whatever far away from the root, the value for stress decreased by a gentle slope. As predicted, when the propellers' thrust reaches the maximum value, the propellers' blade has deformed in the direction of the load vector. The highest value for strain and stress occurs (bollard pull(j=0)) due to thrust and torque values. As shown in Figure 9, in the Bullard states' (j=0) maximum stress is about S=3 Mpa, but for another advance coefficient, this value is about S=1-2 Mpa.

Preprints (www.preprints.org) | NOT PEER-REVIEWED | Posted: 27 January 2021 doi:10.20944/preprints202101.0556.v1

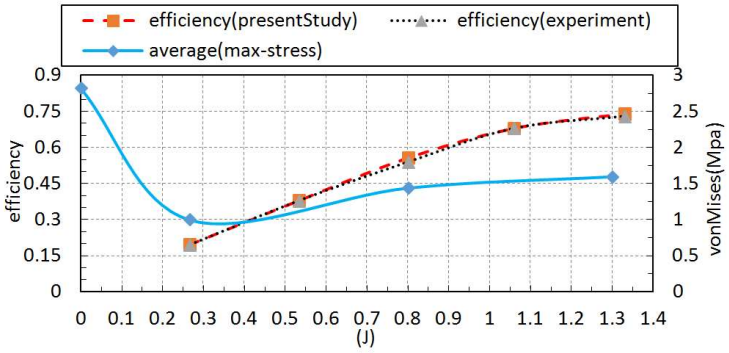

Figure 9. the comparison between maximum stress and hydrodynamic efficiency

3.3. structural Behavior Of propellers' blade

the propellers' work conditions indicate that the blades should sufficiently withstand long work cycles without failure or permanent distortion. The initial research on the propeller's structure and the analysis method was introduced by Taylor [36]. Since then, research on propellers' hydro-elastic Analysis started to include the deformations of the (high-skew) bronze propeller in the 1980s. The marine propeller's design with the systematic propeller series was performed by Ekinci [37], who investigated B-series propellers using some empirical methods with different load conditions. The superiority of the present method is related to perform a quick structural calculation. Indeed, CFD and FEM are not correlating with each other, and the emphasis is put on using one hydrodynamic calculation for the several structural solvers. Different tests could be performed for different materials involved in alloy or composite. A reasonable method to judge how the materials affect the propellers' structures elaborate on two main structural variables, stress and strain. The discrepancy in value and the maximum or minimum occurrence positions are the most important factors in evaluating the propeller's strength. To cast light on the mechanism whereby how the efficient case selected, The maximum Von-Mises stress imposed on the vp1304 use as a key factor to illustrate the stress distribution for each advance coefficient.

For further explanation, some diagrams are used to show the manner of maximum deformation velocity, strain, and Von-Mises stress. In Figure 10, Maximum stress locations are different for each advance coefficient; for instance, at J=1.23, the maximum value for Von-Mises stress is about S=5.2 Mpa, occurred at T=0.08[(rev- 1/(t=0.66s to t=0.12s)], this value is different for J=0.8, maximum Von-Mises stress appears at T=0.12s(end of the rev-1). Such different trends are true for other advanced coefficients. Some oscillation occurs for Von-Mises stress due to neglecting The damping and added mass effects for structural Behavior. For better orientation, Figure 11 shows the stress for one rotation versus The advance coefficient (J), which is a function of the inlet velocity For a constant rotational speed. The blade thickness near the Hub is bigger than the tip; thus, The stresses are bigger at the blade-hub intersection. As can be seen, the Von-Mises range is between ($S=(1.8\text{-}2.4)10^6$) except for T=0.12s ($S=(8.2)10^6$), but the difference is how these values spread on the blades' surface and which blade absorb the maximum load.

Preprints (www.preprints.org) | NOT PEER-REVIEWED | Posted: 27 January 2021 doi:10.20944/preprints202101.0556.v1

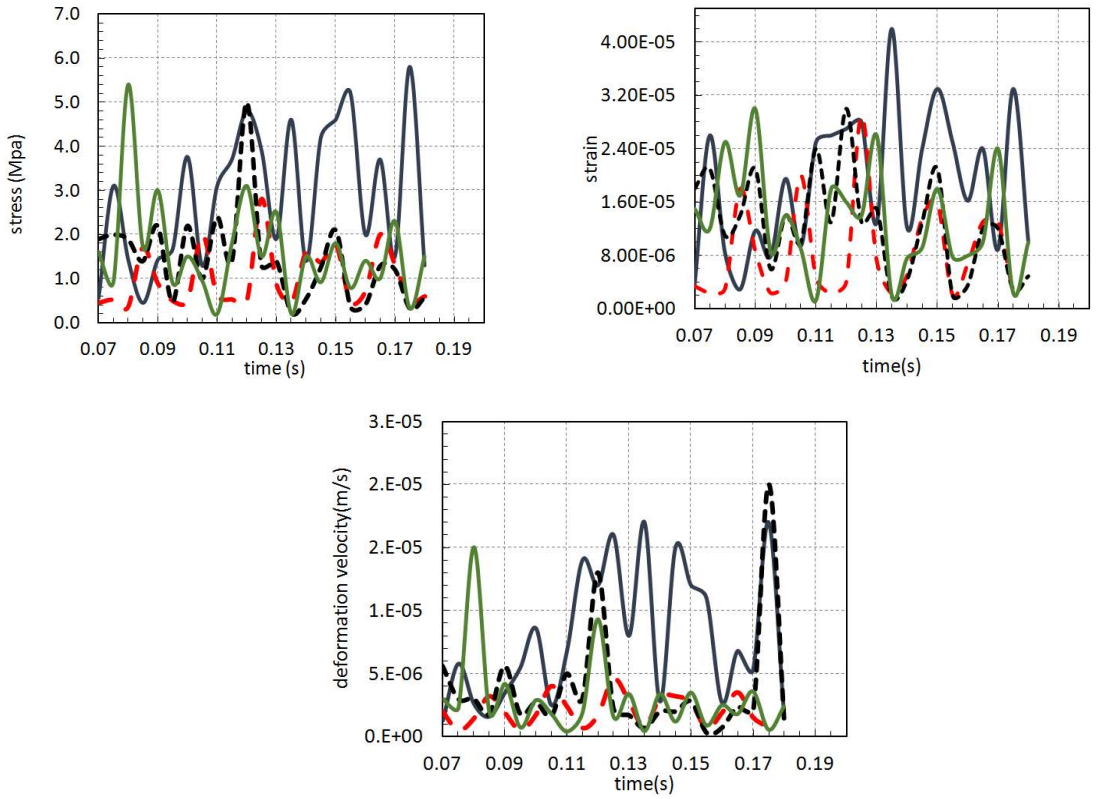

Figure 10. maximum values of three main structural parameters for two rev, at J=0, 0.266, 0.8, 1.23.

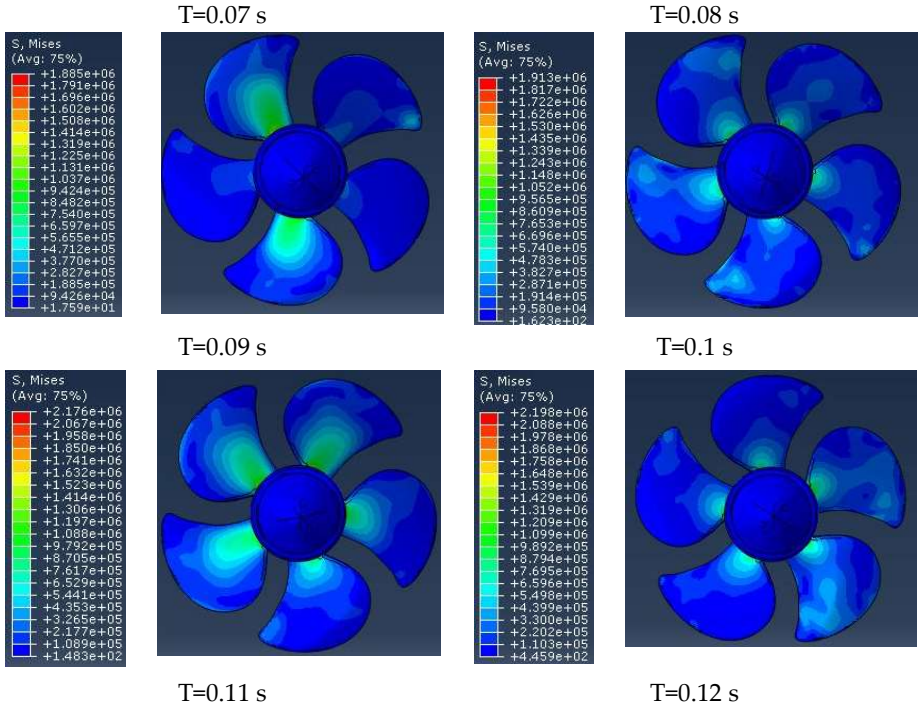

Preprints (www.preprints.org) | NOT PEER-REVIEWED | Posted: 27 January 2021 doi:10.20944/preprints202101.0556.v1

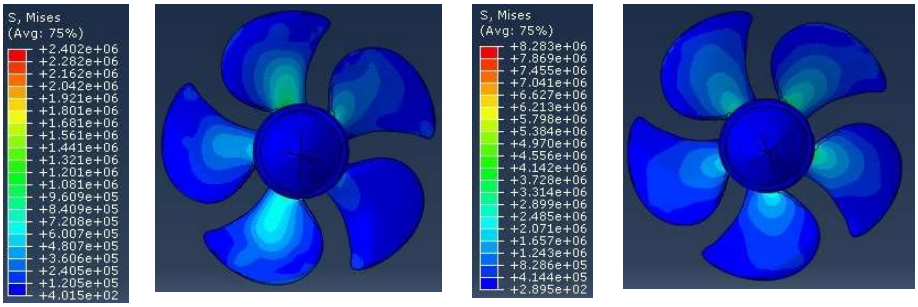

Figure 11. propeller blades' Von-Mises stress contour at different time-Steps

3.4. Propellers' Structural Behavior In Rotation

Three different points on a blade are considered to evaluate the blade rotation angle's effect on Von-Mises stress. The initial impression from Figure 13 is that the point near the blade's root(P1), apart from the advance coefficient, has the highest Von-Mises stress value. And The minimums value belongs to the point at the top of the blade(P3). Albeit, the diagrams' harmony for P1-P2-P3 is similar to each other. Consequently, a set of different graphs for each advance coefficient are used to illustrate how three points on the propeller blade's surface are changed. Following the same approach, The Von-Mises stress versus the rotation angle is shown in Figure 12 for four different advance coefficients. Although The Von-Mises diagrams for all advance coefficients (J) do not have a harmonic trend (rev1: 0-360 & rev 2: 360- 720), the diagram for J=0.266 is more harmonic than others at the same condition. j=0.266 is a minimum point for the stress diagram; thus, the propeller's structural Behavior is more stable and has a minimum value because of maximum k_t and k_q that are occurred at j=0.266. Therefore, the main portion of exerted pressure on the propeller uses to generate thrust.

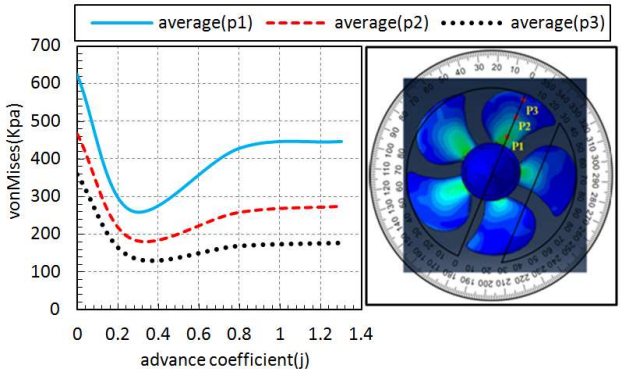

Figure 12. maximum Von-Mises stress at three points on a blade versus advance coefficient

Preprints (www.preprints.org) | NOT PEER-REVIEWED | Posted: 27 January 2021 doi:10.20944/preprints202101.0556.v1

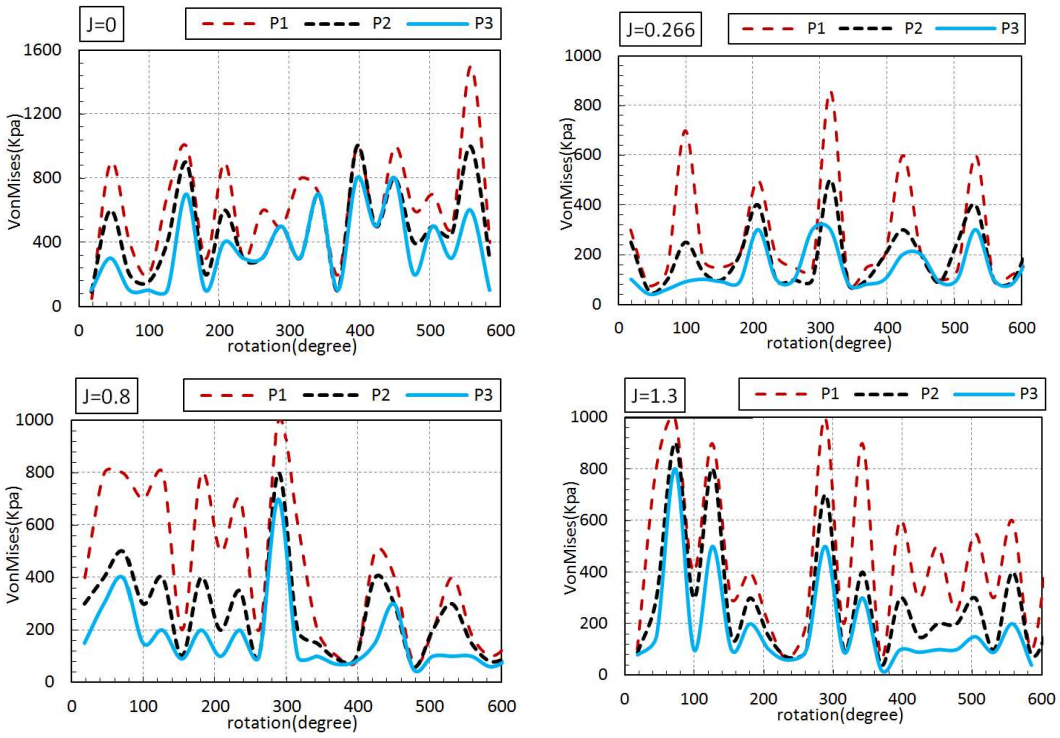

Figure 13. maximum Von-Mises stress at three points versus rotation angle for j=0, 0.266, 0.8, 1.23

4. Conclusion

In the present study, simple surrogate modeling for rigid/quasi-static approach is used to investigate hydroelastic simulation for open water propeller test cases (PPTC); on that basis, CFD-FEM solutions are used distinctly. In the first step, the hydrodynamic solver (InterDyMFoam) is verified with an experimental study. The average efficiency error for different advanced coefficient was about e=3.85%. However, the Thrust and Torque coefficient's error was slightly more than e=8.2% and e=7.2% on average, respectively. Moreover, Hydrodynamic forces and pressures on blades are calculated for each advanced coefficient. After that, pressure and velocity contours versus different advance speeds were demonstrated.

For the second step, The pressure distributions were obtained from OpenFOAM visualization software(ParaView) and used as the initial structural loads in Abaqus software. The key point is, the propeller must have an appropriate rotational motion at each time-step; this procedure continued until it reaches two complete revolutions. Emphasis is put on Von-Mises stress, which is vital for evaluating the propeller's structural strength. Thus, the diagrams and contours are formed based on it. A fact that is borne out is that maximum stress occurred at the bollard pull state(J=0), while apart from the advance coefficient, j=0.266 has the minimum value. Moreover, the value for Von-Mises stress remained stable without a notable change after J=0.8. Concerning the value and the mechanism whereby maximum stress occurred for each advance coefficient could be different for any propellers with varying work conditions. Consequently, the propeller's structural Behavior can effectively analyze by the present method for choosing proper material and design characteristics with a low cost and high precision.

abbreviations

Arbitrary Mesh Interface	AMI
Boundary element Method	BEM
Computational Fluid Dynamic	CFD
Fluid-Structure Interaction	FSI
Finite Element Method	FEM
The International Towing Tank Conference	ITTC
Large Eddy Simulation	LES
Multi Reference Frame	MRF
Pressure Implicit with Splitting of Operators	PISO
Potsdam propeller test case	PPTC
Vortex Lattice Method	VLM
Volume Of Fluid	VOF
Reynolds averaged Navier Stokes	RANS
Rigid/Quasi-Static	RQS
Semi-Implicit Method for Pressure-Linked Equations	SIMPLE
Turbulent Kinetic Energy	TKE

Nomenclature

K_t	Thrust coefficient
K_q	Torque coefficient
V_a	Advance velocity
η	efficiency
J	Advance coefficient
E	elasticity
ρ	density
υ	Poissons' ratio
ω	Angular frequency
S	Von-Mises stress
P_i	Pressure gauge (i=1-2-3)
ε	strain
F	Force
T,t	time
e	Error percentage
rev	Propeller revolution

Reference

1. Young, Y.L. *Hydroelastic behavior of flexible composite propellers in wake inflow*. in *16th international conference on composite materials*. 2007.
2. Olsen, A.S., *Optimisation of propellers using the vortex-lattice method*. 2002.
3. Cokljat, D., et al. *Embedded LES methodology for general-purpose CFD solvers*. in *Sixth International Symposium on Turbulence and Shear Flow Phenomena*. 2009. Begel House Inc.
4. Yao, J., *Investigation on hydrodynamic performance of a marine propeller in oblique flow by RANS computations.* International Journal of Naval Architecture and Ocean Engineering, 2015. **7**(1): p. 56-69.
5. Krasilnikov, V., Z. Zhang, and F. Hong. *Analysis of unsteady propeller blade forces by RANS*. in *First international symposium on marine propulsors smp*. 2009.
6. Dubbioso, G., R. Muscari, and A. Di Mascio, *Analysis of a marine propeller operating in oblique flow. Part 2: very high incidence angles.* Computers & Fluids, 2014. **92**: p. 56-81.
7. Abdel-Maksoud, M., K. Hellwig, and J. Blaurock. *Numerical and experimental investigation of the hub vortex flow of a marine propeller*. in *25th Symposium on Naval Hydrodynamics, St. John's, Newfoundland-Labrador, Canada*. 2004.
8. Simonsen, C.D. and F. Stern, *RANS maneuvering simulation of Esso Osaka with rudder and a body-force propeller.* Journal of Ship Research, 2005. **49**(2): p. 98-120.
9. Valentine, D.T., *Reynolds-averaged navier-stokes codes and marine propulsor analysis*. 1993, NAVAL SURFACE WARFARE CENTER CARDEROCK DIV BETHESDA MD HYDROMECHANICS ….
10. Das, H. *CFD Analysis for Cavitation of a Marine Propeller*. in *Proceedings of the 8th Symposium on High Speed Marine Vehicles*. 2008.
11. Mulcahy, N., B. Prusty, and C. Gardiner, *Hydroelastic tailoring of flexible composite propellers.* Ships and Offshore structures, 2010. **5**(4): p. 359-370.
12. Blasques, J.P., C. Berggreen, and P. Andersen, *Hydro-elastic analysis and optimization of a composite marine propeller.* Marine Structures, 2010. **23**(1): p. 22-38.
13. Lee, H., et al., *Hydro-elastic analysis of marine propellers based on a BEM-FEM coupled FSI algorithm.* International journal of naval architecture and ocean engineering, 2014. **6**(3): p. 562-577.
14. He, X., Y. Hong, and R. Wang, *Hydroelastic optimisation of a composite marine propeller in a non-uniform wake.* Ocean engineering, 2012. **39**: p. 14-23.
15. Maljaars, P., et al., *Experimental validation of fluid–structure interaction computations of flexible composite propellers in open water conditions using BEM-FEM and RANS-FEM methods.* Journal of Marine Science and Engineering, 2018. **6**(2): p. 51.
16. Vassen, J.-M., et al., *Strong coupling algorithm to solve fluid-structure-interaction problems with a staggered approach.* ESASP, 2011. **692**: p. 128.

17. Benra, F.-K., et al., *A comparison of one-way and two-way coupling methods for numerical analysis of fluid-structure interactions.* Journal of applied mathematics. **2011**.
18. Piro, D.J., *A Hydroelastic Method for the Analysis of Global Ship Response Due to Slamming Events*. 2013.
19. Moukalled, F., L. Mangani, and M. Darwish, *The finite volume method in computational fluid dynamics*. Vol. 6. 2016: Springer.
20. Aagaard, O., *Hydroelastic analysis of flexible wedges*. 2013, Institutt for marin teknikk.
21. Taylor, D., *The Speed and Power of Ships. Ransdell.* Inc., Washington, DC, 1933.
22. Cohen, J.W., *On stress calculations in helicoidal shells and propeller blades.* 1955.
23. Conolly, J., *Strength of propellers.* Trans RINA, 1974. **103**: p. 139-204.
24. Young, Y.L., *Fluid–structure interaction analysis of flexible composite marine propellers.* Journal of fluids and structures, 2008. **24**(6): p. 799-818.
25. Greening, P.D., *Dynamic finite element modelling and updating of loaded structures*. 1999, University of Bristol Bristol.
26. Taghipour, R., *Efficient prediction of dynamic response for flexible and multi-body marine structures.* 2008.
27. Barkmann, U., H.-J. Heinke, and L. Lübke. *Potsdam propeller test case (PPTC)*. in *Proceeding of the Second International Symposium on Marine Propulsorssmp'11*. 2011.
28. Gornicz, T. and J. Kulczyk, *The Assessment of the Application of the CFD Package OpenFOAM to Simulating Flow around the Propeller.* Marine Navigation and Safety of Sea Transportation: Maritime Transport & Shipping, 2013. **247**.
29. Cosden, I.A. and J.R. Lukes, *A hybrid atomistic–continuum model for fluid flow using LAMMPS and OpenFOAM.* Computer Physics Communications, 2013. **184**(8): p. 1958-1965.
30. Klasson, O.K. and T. Huuva. *Potsdam propeller test case (PPTC)*. in *Second International Symposium on Marine Propulsors, SMP*. 2011.
31. Khan, A.M., *Flexible composite propeller design using constrained optimization techniques.* 1997.
32. Barlow, J., *Optimal stress locations in finite element models.* International Journal for Numerical Methods in Engineering, 1976. **10**(2): p. 243-251.
33. Barlow, J., *More on optimal stress points—reduced integration, element distortions and error estimation.* International Journal for Numerical Methods in Engineering, 1989. **28**(7): p. 1487-1504.
34. Panciroli, R., *Dynamic Failure of Composite and Sandwich Structures, vol. 192*. 2013, Dordrecht: Springer Netherlands.
35. Heller, S. and N. Jasper, *On the structural design of planing craft.* Quarterly Transactions, RINA. July, 1960.
36. Taylor, J.L., *Natural Vibration Frequencies of Flexible Rotor Blades.* Aircraft Engineering and Aerospace Technology, 1958.
37. Ekinci, S., *A practical approach for design of marine propellers with systematic propeller series.* Brodogradnja: Teorija i praksa brodogradnje i pomorske tehnike, 2011. **62**(2): p. 123-129.